

Supporting information

Polyesteramide library from dicarboxylic acids and 2,2' bis(2 oxazoline): Synthesis, characterization, nanoparticle formulation and molecular dynamic simulations

Irina Muljajew,^{†,‡} Andreas Erlebach,^{‡,§} Christine Weber,^{†,‡} Johannes R. Buchheim,[&] Marek Sierka,^{‡,§} Ulrich S. Schubert^{†,‡,}*

[†]Laboratory of Organic and Macromolecular Chemistry (IOMC), Friedrich Schiller University Jena, Humboldtstr. 10, 07743 Jena, Germany

[‡]Jena Center for Soft Matter (JCSM), Friedrich Schiller University Jena, Philosophenweg 7, 07743 Jena, Germany

[§]Otto Schott Institute of Materials Research (OSIM), Friedrich Schiller University Jena, Lößdergraben 32, 07743 Jena, Germany

[&]Institute for Technical Chemistry and Environmental Chemistry, Center for Energy and Environmental Chemistry Jena (CEEC Jena), Friedrich Schiller University Jena, Philosophenweg 7a, 07743 Jena, Germany

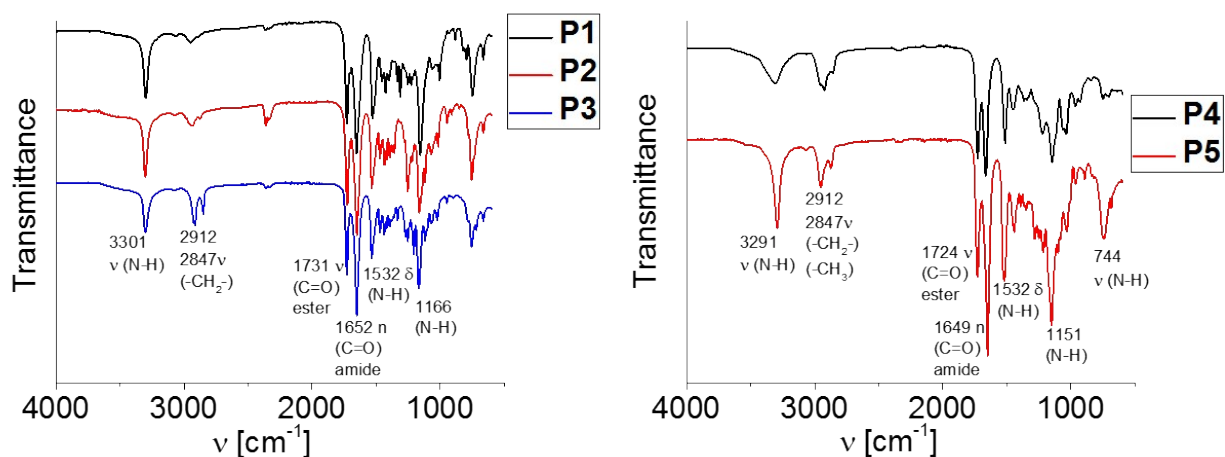


Figure S1: FT-ATR-IR spectra of the polyestaramides **P1** to **P5**.

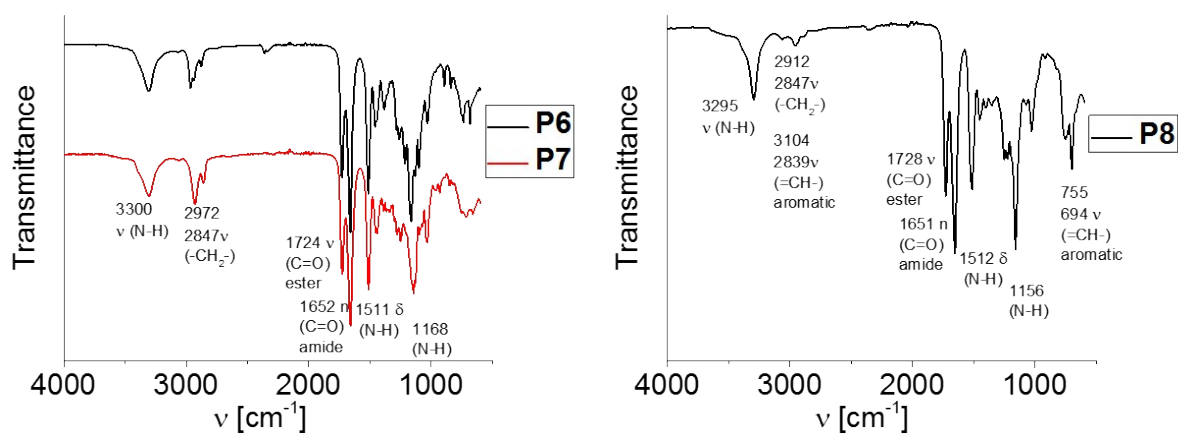


Figure S2: FT-ATR-IR spectra of the polyestaramides **P6** to **P8**.

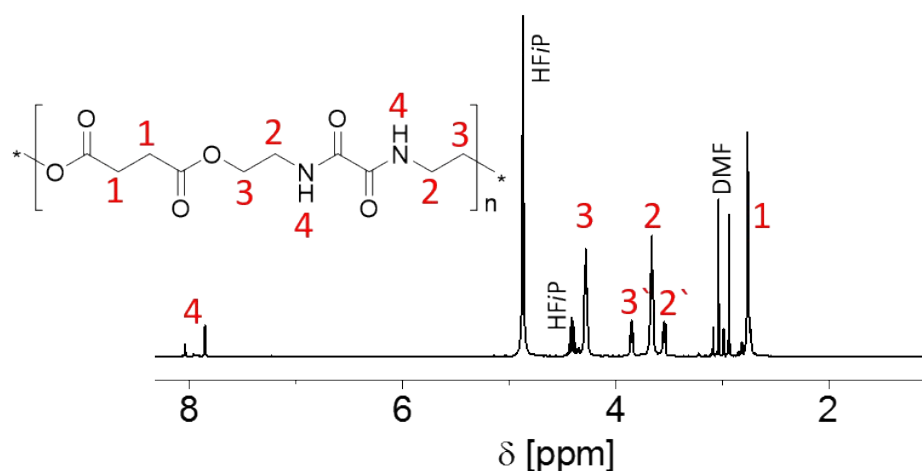


Figure S3: ^1H NMR spectrum (400 MHz, HF*i*P- d_2) of **P1** and assignment of the peaks to the schematic representation of the polymer structure. Peaks 3' and 2' correspond to the chemical shift of a polymer end group $-\text{CONH}-\text{CH}_2-\text{CH}_2-\text{OH}$.

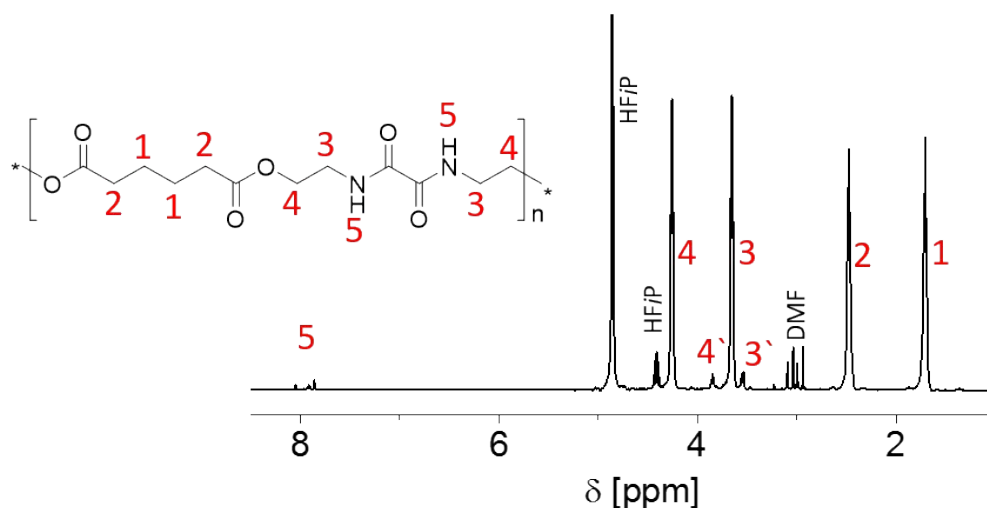


Figure S4: ^1H NMR spectrum (400 MHz, HF*i*P- d_2) of **P2** and assignment of the peaks to the schematic representation of the polymer structure. Peaks 4' and 3' correspond to the chemical shift of a polymer end group $-\text{CONH}-\text{CH}_2-\text{CH}_2-\text{OH}$.

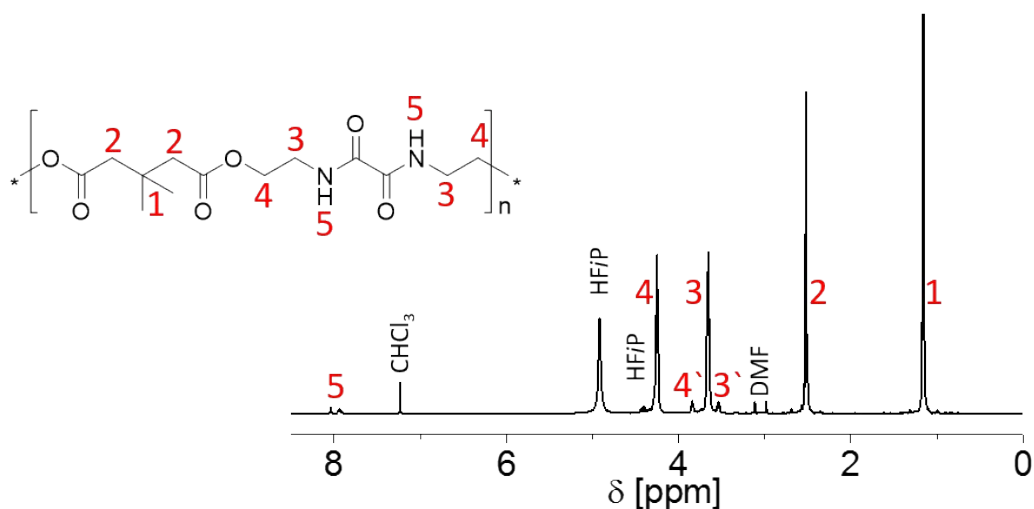


Figure S5: ^1H NMR spectrum (400 MHz, HFIP- d_2) of **P4** and assignment of the peaks to the schematic representation of the polymer structure. Peaks 4' and 3' correspond to the chemical shift of a polymer end group $-\text{CONH}-\text{CH}_2-\text{CH}_2-\text{OH}$.

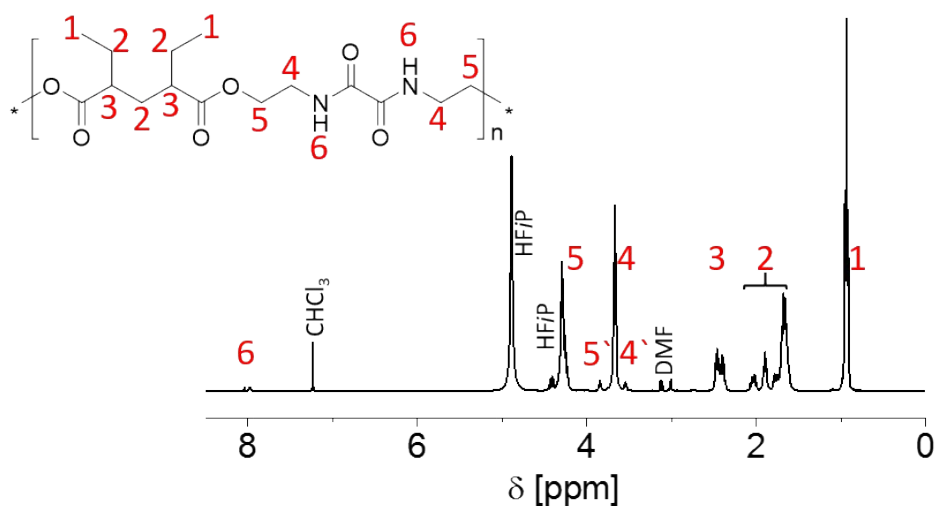


Figure S6: ^1H NMR spectrum (400 MHz, HFIP- d_2) of **P5** and assignment of the peaks to the schematic representation of the polymer structure. Peaks 5' and 4' correspond to the chemical shift of a polymer end group $-\text{CONH}-\text{CH}_2-\text{CH}_2-\text{OH}$.

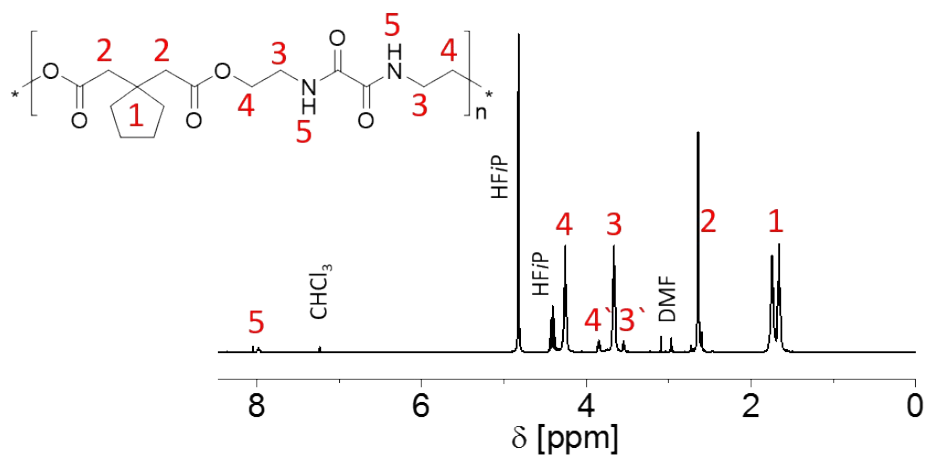


Figure S7: ¹H NMR spectrum (400 MHz, HF*i*P-d₂) of **P6** and assignment of the peaks to the schematic representation of the polymer structure. Peaks 4' and 3' correspond to the chemical shift of a polymer end group -CONH-CH₂-CH₂-OH.

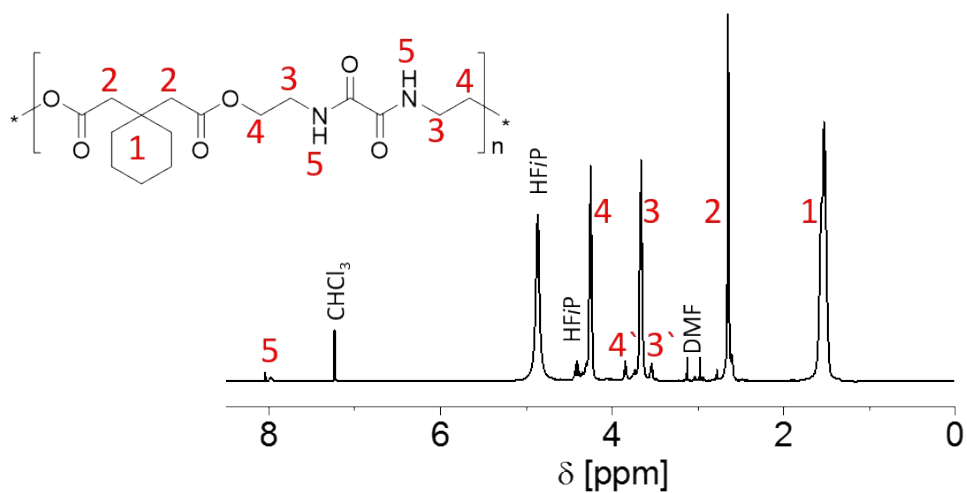


Figure S8: ¹H NMR spectrum (400 MHz, HF*i*P-d₂) of **P7** and assignment of the peaks to the schematic representation of the polymer structure. Peaks 4' and 3' correspond to the chemical shift of a polymer end group -CONH-CH₂-CH₂-OH.

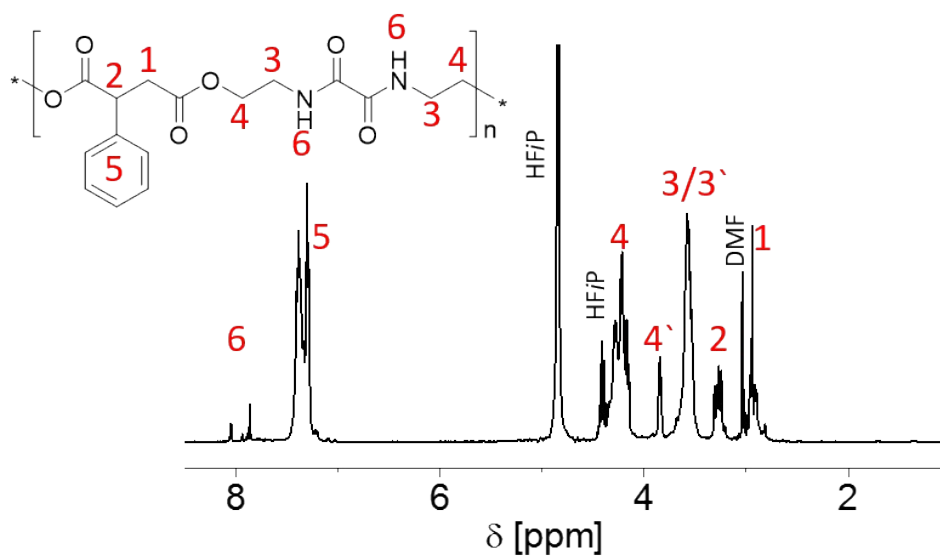


Figure S9: ^1H NMR spectrum (400 MHz, HFIP- d_2) of **P8** and assignment of the peaks to the schematic representation of the polymer structure. Peaks 4' and 3' correspond to the chemical shift of a polymer end group $-\text{CONH}-\text{CH}_2-\text{CH}_2-\text{OH}$.

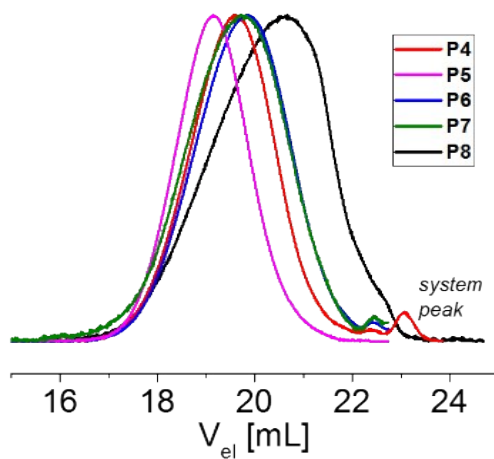


Figure S10: SEC elugrams (DMAc, RI detection) of the polyesters **P4** to **P8**.

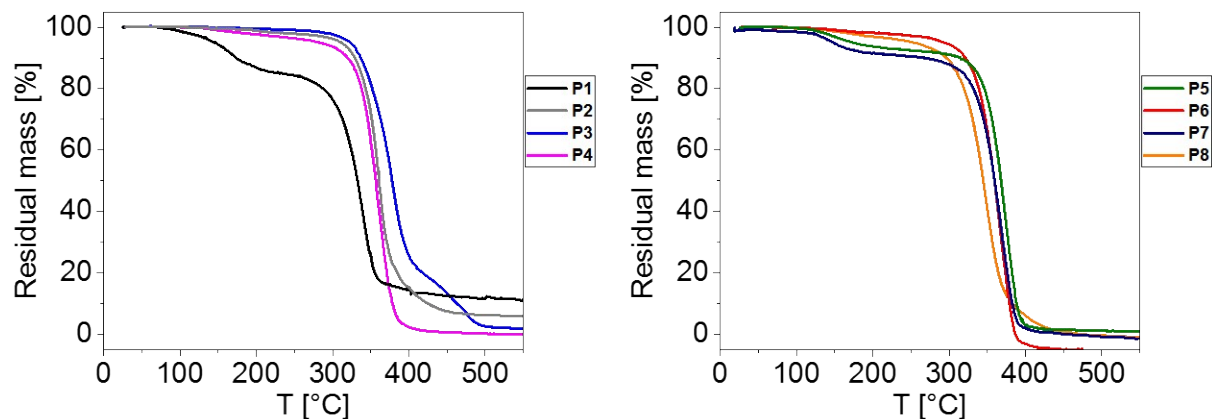


Figure S11: TGA thermograms of **P1** to **P4** (left) and **P5** to **P8** (right) (N₂ atmosphere, heating rate 20 K min⁻¹). The mass loss below 200 °C was due to residual DMF present in **P1**, **P7** and **P5**.

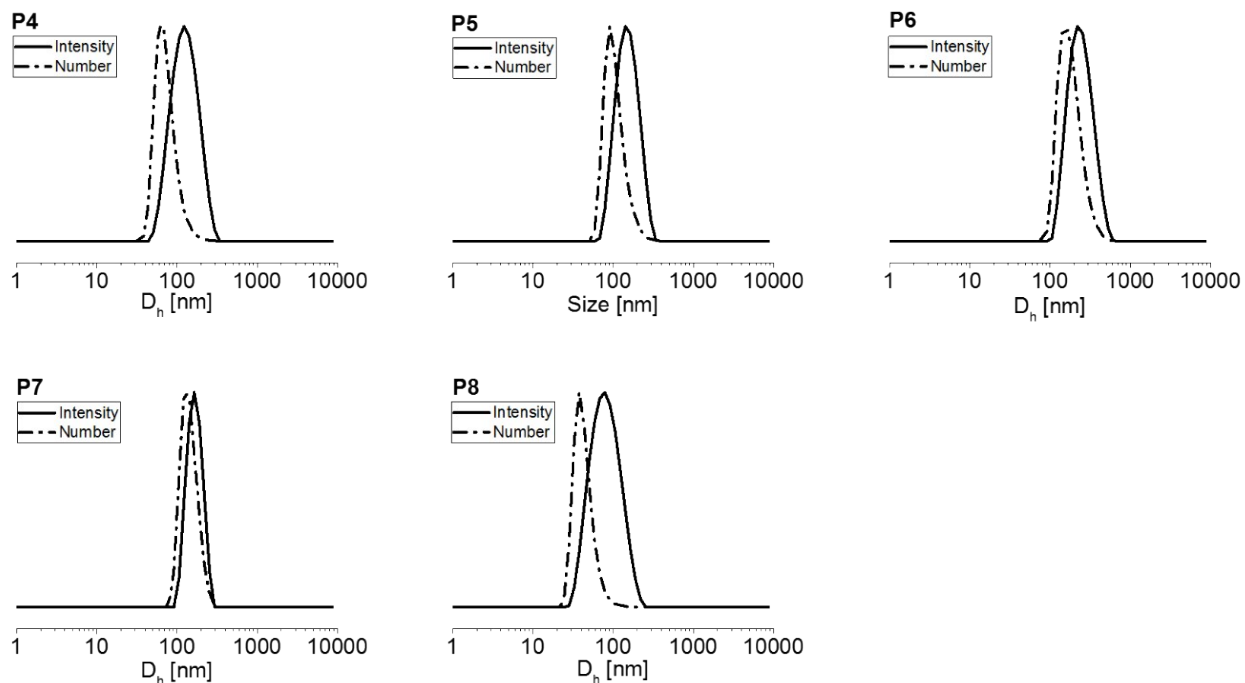


Figure S12: DLS size distributions of the nanoparticles prepared from **P3** to **P8**. The full lines represent the intensity-weighted data, the dotted lines represent the number-weighted data.

Additional information to WAXS investigations:

P1: The material crystallized in the α -form. The reflection positions were $2\theta = 18.3^\circ$ ($d = 4.81 \text{ \AA}$), $2\theta = 20.8^\circ$ ($d = 4.25 \text{ \AA}$), $2\theta = 23.2^\circ$ ($d = 3.85 \text{ \AA}$) and a shoulder with the Bragg-Reflex $2\theta = 24.7^\circ$ ($d = 3.66 \text{ \AA}$). From this, the primitive unit cell was determined with the following parameters:

Lattice parameter	Experimental value	Calculated value structure IIIa	Refined value
a [\AA]	4,96	8.886	8.414
b [\AA]	10,86	9.337	9.952
c [\AA]	22,7	31.272	33.267
α [$^\circ$]	51	89.7	78.6
β [$^\circ$]	77	88.3	84.6
γ [$^\circ$]	60	68.0	60.9

The degree of crystallization was about 50%.

P3: The material included an α - and δ -modification. The Bragg reflections of the α -phase were $2\theta = 19.7^\circ$ ($d = 4.50 \text{ \AA}$) and $2\theta = 23.2^\circ$ ($d = 3.83 \text{ \AA}$). The δ phase was identified by the Bragg angle $2\theta = 21.4^\circ$ ($d = 4.15 \text{ \AA}$). From this, the primitive unit cells were determined with the following parameters:

Lattice parameter	α -Phase	δ -Phase
a	5,17 \AA	4,79 \AA
b	10,8 \AA	4,79 \AA
c	21,7 \AA	112,8 \AA
α	51°	90°
β	77°	90°
γ	61°	90°

The α -phase thus has a preferred (100) orientation and growth of the crystals. The degree of crystallization was about 39%.

Construction of initial crystal structure models for **P1** is shown in **Figure S13**. Three chain conformations were tested using a chain fragment containing two repeating units with every atom in plane (**I**), with rotation of the alkaline spacer and ester groups by 90° in the same (**II**) and opposite direction (**III**). After geometry optimization of **I-III**, 4 chain fragments were placed into an orthorhombic unit cell with lattice parameters of 7.0, 35.1 and 10.5 Å for *a*, *b* and *c* axis, respectively. In addition, a parallel (*e.g.*, **Ip**) and antiparallel (*e.g.*, **Ia**) chain alignment (**Figure S13b** and **S13c**) as well as a shift of the polymer chains along the along *b* axis by about 10 Å (*e.g.*, **Ip_b**) and along the *c* axis by about 3.5 Å (*e.g.*, **Ip_c**) was tested. As in case of **Iabc**, most of the optimized crystal structures show the diffraction peak with highest intensity at 2θ of 26.3° not present in experimentally determined diffractogram. In contrast, **IIIa** and **IIac** reveal the main diffraction peaks below $2\theta = 25^\circ$. Therefore, these structure models were chosen for Rietveld refinement.

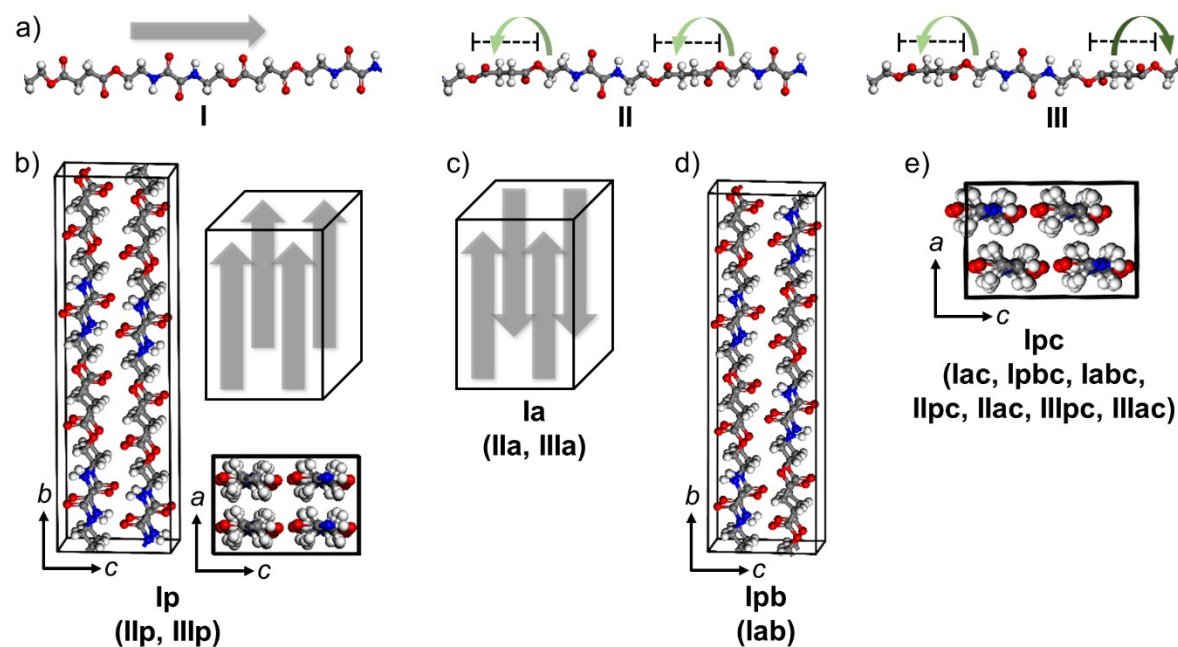


Figure S13: Construction of initial structure models of **P1** using a) different chain conformations (**I**, **II**, **III**), b) parallel (**p**) or c) antiparallel (**a**) alignment in the orthorhombic unit cell as well as d) shifted polymer chains along the *b* (**b**) or e) *c* (**c**) axis. Notations of other initial structure models not shown are given in brackets. C: grey, O: red, H: white.

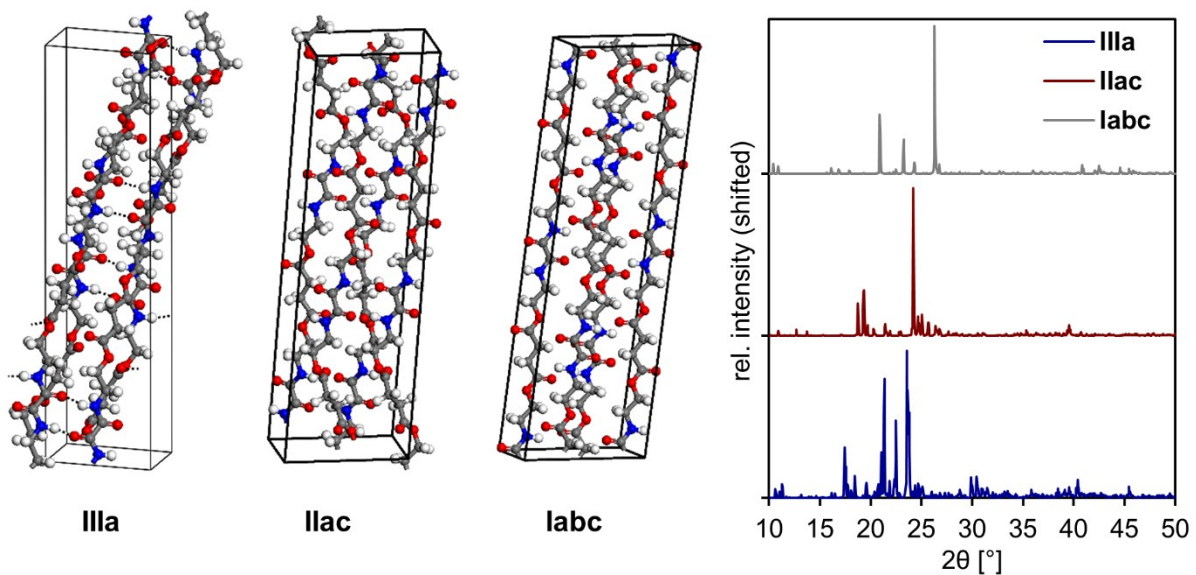


Figure S14: Geometrically optimized crystal structures (a) used for Rietveld refinement of experimentally determined diffractogram and calculated X-ray diffraction patterns (b) of **P1** (C: grey, O: red, H: white).

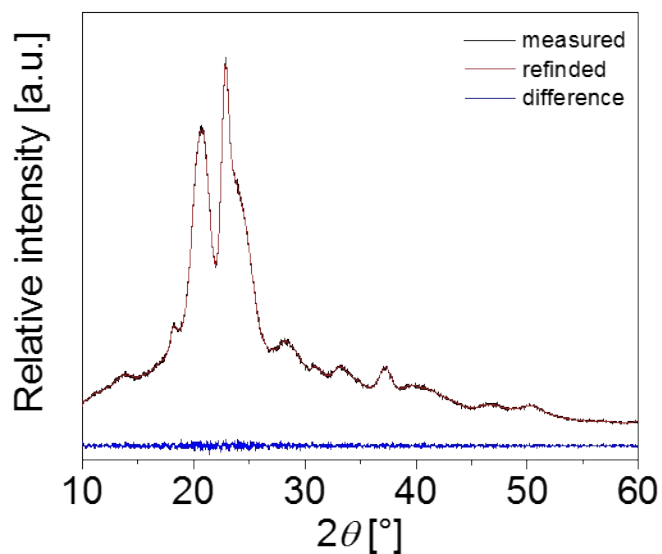


Figure S15: Rietveld structure refinement of the measured diffractogram of **P1** with the calculated diffractogram based on structure **IIIa**.

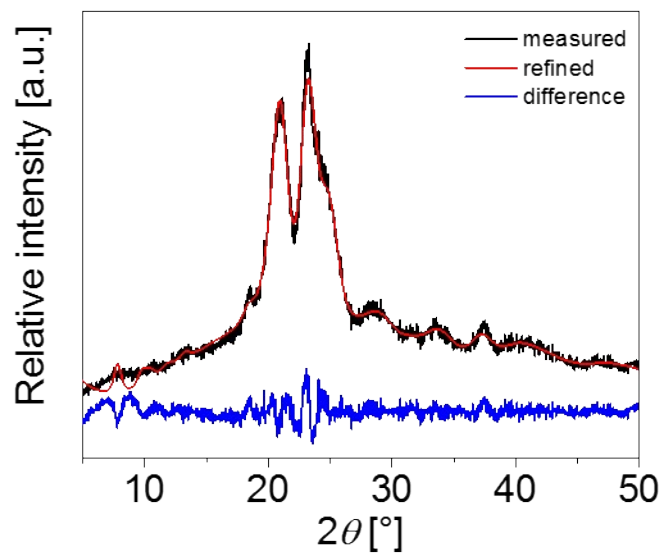


Figure S16: Rietveld structure refinement of the measured diffractogram of **P1** with the caclulated diffractogram based on structure **IIac**.

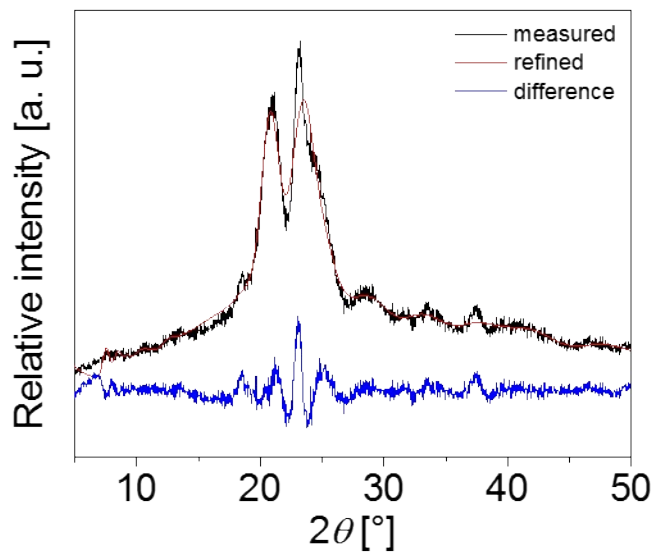


Figure S17: Rietveld structure refinement of the measured diffractogram of **P1** with the caclulated diffractogram based on structure **Iabc**.

The average potential energy per segment e for an amorphous solid consisting of segments with a radial distribution function $g_{ij}(r)$ interacting through a pair potential $\phi_{ij}(r)$ is given as¹

$$e = \frac{\varrho}{2} \sum_{i=1}^c \sum_{j=1}^c x_i x_j \int_0^{\infty} \phi_{ij}(r) 4\pi r^2 g_{ij}(r) dr, \quad (\text{S1})$$

where c denotes different components with segment fractions x , the segment density ϱ and the center-to-center distance r between two segments. Here, one segment is defined as one polymer repeating unit or solvent molecule. $\phi_{ij}(r)$ assumes the functional form of a square well potential, with

$$\phi_{ij}(r) = \begin{cases} \infty, & r < r_0 \\ \varepsilon_{ij}, & r_0 \leq r \leq r_1 \\ 0, & r > r_1. \end{cases} \quad (\text{S2})$$

Figure S18 shows the radial distribution function determined for pure THF along with the corresponding pair potential. Using this form of potential function, the evaluation of the integral in Eqn. S1 can be limited to the interval $[r_0, r_1]$ with the distance independent interaction energy ε_{ij} since $g_{ij}(r) = 0$ for $r < r_0$ and $\phi_{ij}(r) = 0$ for $r > r_1$. Therefore, Eqn. S1 can be rewritten using Eqn. S2 and $\varrho_j = x_j \varrho$ as

$$e = \frac{1}{2} \sum_{i=1}^c \sum_{j=1}^c x_i \varepsilon_{ij} \varrho_j \int_{r_0}^{r_1} 4\pi r^2 g_{ij}(r) dr. \quad (\text{S3})$$

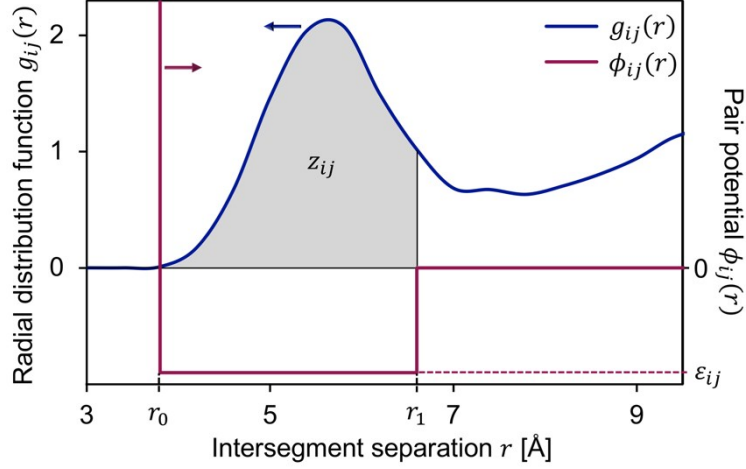


Figure S18: Radial distribution function $g_{ij}(r)$ determined for pure THF along with the corresponding square well potential $\phi_{ij}(r)$ (Eqn. S2). The shaded area represents the integral used for calculation of the coordination number z_{ij} (Eqn. S4).

The coordination number z_{ij} is defined as the average number of segments j surrounding segments i in a spherical shell ranging from r_0 to r_1

$$z_{ij} = \rho_j \int_{r_0}^{r_1} 4\pi r^2 g_{ij}(r) dr, \quad (\text{S4})$$

Using z_{ij} for a pure (p) amorphous solid solely containing segments i Eqn. S3 simplifies to

$$e_{i,p} = \frac{z_{ii,p}}{2} \epsilon_{ii}. \quad (\text{S5})$$

Similarly, defining an average coordination number $\bar{z}_{12} = x_1 z_{12} + x_2 z_{21}$ between unlike segments i - j , Eqn. S3 for a binary mixture (m) simplifies to

$$e_m = \frac{1}{2} (x_1 z_{11,m} \epsilon_{11} + x_2 z_{22,m} \epsilon_{22} + \bar{z}_{12} \epsilon_{12}). \quad (\text{S6})$$

The parameter r_1 used for calculation of z_{ij} (Eqn. S4) corresponds to the diameters of spheres with volumes v_i and v_m , which are the average segment volumes obtained from atomistic simulations of the pure components and the mixture, respectively. Inserting Eqns. S5 and S6 into the general definition of the energy of mixing per segment Δe_m

$$\Delta e_m = e_m - x_1 e_{1,p} - x_2 e_{2,p}, \quad (\text{S7})$$

yields the energy of mixing $\Delta e_{m,z}$ as a function of the coordination number changes of mixing $\Delta z_i = z_{ii,m} - z_{ii,p}$

$$\Delta e_{m,z} = \frac{1}{2}(x_1 \Delta z_1 \varepsilon_{11} + x_2 \Delta z_2 \varepsilon_{22} + \bar{z}_{12} \varepsilon_{12}). \quad (\text{S8})$$

For both Δz_i and \bar{z}_{12} quadratic composition dependency is assumed with the functional forms

$$\Delta z_i = A_i(1 - x_i)^2 + B_i(1 - x_i), \quad (\text{S9a})$$

$$\bar{z}_{12} = 2A_{12}x_1x_2. \quad (\text{S9b})$$

Figure S19 shows the composition dependence of Δz_i and \bar{z}_{12} calculated for the mixture containing **P4** and THF (solid lines). The composition independent parameters A_i and B_i in Eqns. S9a and S9b are obtained using three known values of Δz_i and \bar{z}_{12} at $x_i = 0$, $x_i = 1$ as well as the composition used for the atomistic simulations (squares in Fig. S14). For $x_i \rightarrow 0$, that is infinite dilution of component i , no intermolecular i - i contacts are present in the mixture such that $\Delta z_i \rightarrow -z_{ii,p}$. Similarly, no change of the coordination numbers $\Delta z_i \rightarrow 0$ occurs for mixtures at $x_i \rightarrow 1$. Obviously, \bar{z}_{12} is zero for compositions close to the pure states. In addition, the total coordination number z is shown in Fig. S14, for which applies: $z = x_1 z_{11,m} + x_2 z_{22,m} + \bar{z}_{12}$.

The use of the model functions Eqns. S9a and S9b allows to include the effect of different coordination states of unequal sized segments in the mixture as a function of the composition. In contrast, the Flory-Huggins (FH) theory employs a mean-field approximation with equally sized segments and a composition independent lattice coordination number z_{FH} . Here, z_{FH} is defined as the total coordination number z of the mixture calculated from atomistic simulations. Due to the random occupation of the FH mean-field lattice, the coordination numbers of the mixture are approximated as $\bar{z}_{12} \approx 2x_1x_2z_{FH}$ and $z_{ii,m} \approx x_iz_{FH}$. Since in the FH theory the coordination numbers of the pure states are $z_{ii,p} = z_{FH}$, the coordination number change Δz_i is a linear function of the composition $\Delta z_i \approx z_{FH}(x_i - 1) = -z_{FH}x_j$. Inserting these relations into Eqn. S8 results in the known FH expression for the energy of mixing $\Delta e_{m,FH}$ along with the definition of the FH interaction parameter χ_{FH} (*cf.* Eqns. 1 and 2)²

$$\Delta e_{m,FH} = RTx_1x_2 \frac{z_{FH}}{RT} (\varepsilon_{12} - 0.5(\varepsilon_{11} + \varepsilon_{22})) = RTx_1x_2 \chi_{FH} \quad (S10)$$

Results for the coordination numbers and the energy of mixing for the THF-**P4** mixture using the FH theory are also shown in Fig. S14 (dashed lines).

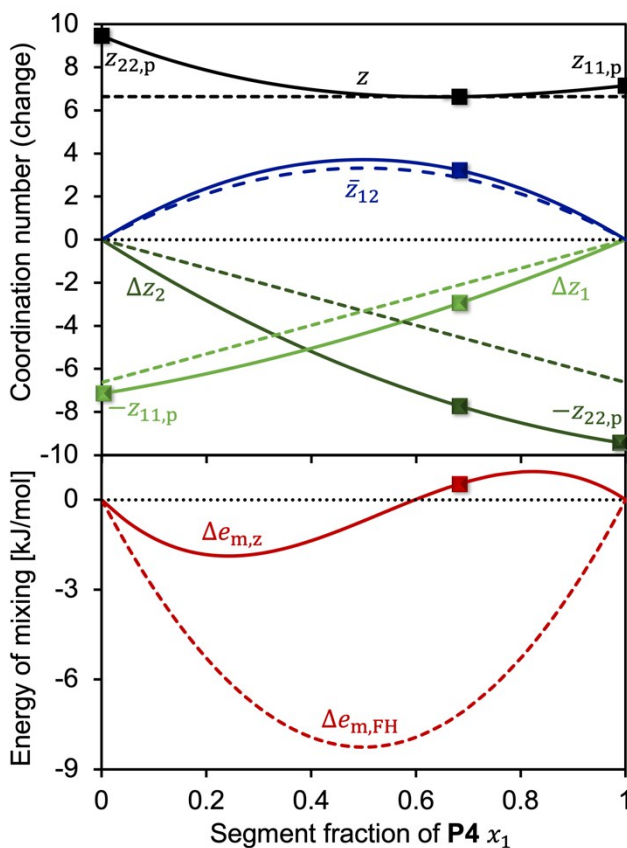


Figure S19: Total coordination number z , coordination number of unlike segments \bar{z}_{12} and the coordination number change of like segments Δz_i (upper part) as well as the energy of mixing Δe_m (lower part) as a function of composition for the mixture THF-**P4**. Solid lines: Model using Eqns. S5-S9, dashed lines: FH theory (Eqn. S10), squares: Values calculated from atomistic simulations.

In order to keep consistency with the FH expression for the entropy of mixing (*cf.* Eqn. 3), equally sized segments are assumed for the mixed state showing the average segment volume of the mixture v_m . However, the effects of unequally sized particles on the lattice coordination number as a function the composition can be considered with a composition dependent FH parameter χ_z . The actual intermolecular structure of the mixture is implicitly included in the mean-field approach

of the FH theory taking a ‘non-randomness’ of the lattice into account. For this, Eqn. S8 is used for calculation χ_z , such that $\Delta e_{m,z} = RTx_1x_2\chi_z$, yielding

$$\chi_z = \frac{1}{RT} \left(\frac{\bar{z}_{12}}{2x_1x_2} \varepsilon_{12} + 0.5 \left(\frac{\Delta z_1}{x_2} \varepsilon_{11} + \frac{\Delta z_2}{x_1} \varepsilon_{22} \right) \right). \quad (\text{S11})$$

Finally, inserting Eqns. S9a and S9b into S11, using $x_1 + x_2 = 1$ and defining the functions $F_i(x_i)$ as well as F_{12}

$$F_i(x_i) = \frac{\Delta z_i}{1 - x_i} = A_i(1 - x_i) + B_i, \quad (\text{S12a})$$

$$F_{12} = \frac{\bar{z}_{12}}{2x_1x_2} = A_{12}, \quad (\text{S12b})$$

results in a linear dependency of the FH parameter χ_z on the composition (*cf.* Eqn. 6)

$$\chi_z = \frac{1}{RT} (F_{12} \varepsilon_{12} + 0.5 (F_1(x_1) \varepsilon_{11} + F_2(x_2) \varepsilon_{22})). \quad (\text{S13})$$

In this work, the calculation of the model parameters required in Eqns. S4-S13 used atomistic simulations providing two central quantities, (*i*) the intermolecular RDF $g_{ij}(r)$ characterizing the amorphous structure and (*ii*) the cohesive energy densities C as measure for the intermolecular interactions. The latter are related to the Hildebrand solubility parameter *via* $\delta = \sqrt{C}$. The RDF $g_{ij}(r)$ required for calculation of z_{ij} (Eqn. S4) are obtained using coarse-grained models of the equilibrated and geometrically optimized (atomistic) structures. The parameter r_0 is defined as intersegment distance at which $g_{ij}(r) > 0$ for $r > r_0$. As mentioned above, for calculation of the coordination numbers between like segments, the diameter of a sphere with volume v_i was chosen for r_1 , which corresponds to the center-to-center distance of two segments in contact. For calculation of \bar{z}_{12} , the average molar volume of the mixture v_m was used.

In addition, δ (or C) is connected with the potential energy (Eqns. S5 and S6) and the molar volumes of the pure states (per segment) v_i^3 by the relation $e_i = -v_i \delta_i^2$. The same relation holds for the potential energy of the mixture $e_m = -v_m \delta_m^2$. Inserting these relations in Eqns. S5-S7 yields Eqns. 4, 5 and 7.

Figure S20 shows the dependence of Δg_m on the polymer segment fraction x_1 for the tested PEA solutions calculated using χ_{FH} and χ_z .

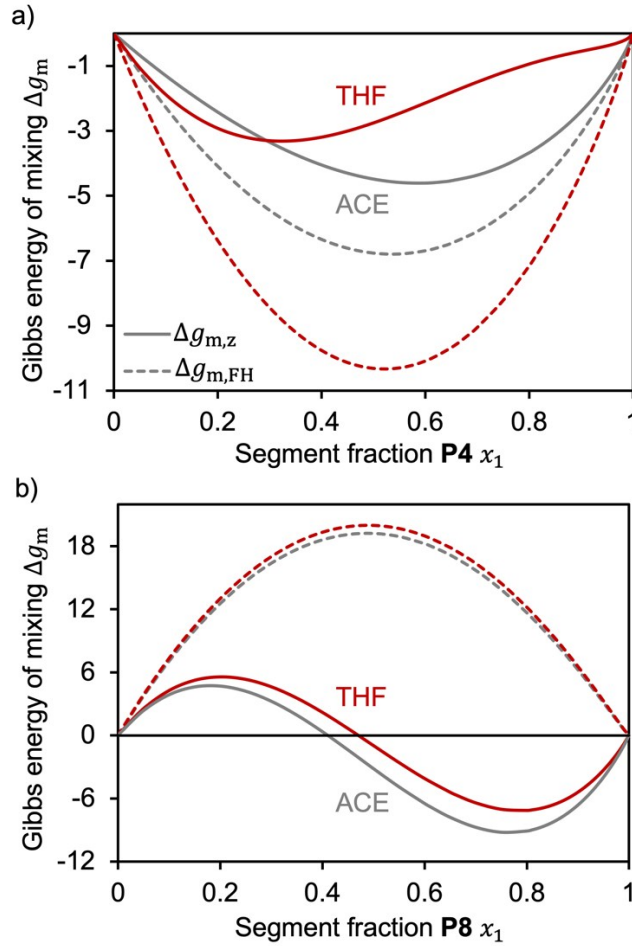


Figure S20: Gibbs energies of mixing Δg_m (Eqn. 3) as a function of the polymer segment fraction x_1 of binary mixtures containing THF (red) and acetone (ACE, gray) as well as (a) **P4** and (b) **P8**, calculated using χ_{FH} (Eqn. 1, dashed lines) and χ_z (Eqn. 6, solid lines).

All model parameters for the pure polymers (**P4**, **P8**) and solvents (THF, ACE) are summarized in **Table S1**. The parameter characterizing the corresponding mixtures are shown in **Table S2**.

Table S1. Hildebrandt solubility parameters δ_i , molar volumes (per segment) v_i , coordination number $z_{ii,p}$ and pair interaction parameter ϵ_{ii} of the pure components.

	P4	P8	THF	ACE
δ_i [MPa ^{0.5}]	20.67	20.75	18.33	19.26
v_i [cm ³ /mol]	247.50	267.06	84.83	74.46

$z_{ii,p}$	7.15	5.09	9.46	8.42
ε_{ii} [kJ/mol]	-29.58	-45.21	-6.03	-6.56

Table S2. Hildebrandt solubility parameters δ_m [MPa^{0.5}], average molar volumes (per segment) v_m [cm³ mol⁻¹], polymer segment fraction x_1 used for atomistic simulations (sim), model parameters for coordination numbers Δz_i and \bar{z}_{12} (Eqn. S9), pair interaction parameters ε_{ij} [kJ mol⁻¹], coordination numbers of the Flory-Huggins (FH) lattice z_{FH} , FH parameters χ_{FH} (Eqns. S10), as well as the energies of mixing Δe_m (Eqns. S8 and S10) [kJ mol⁻¹] obtained for compositions x_1 used in experiments (exp) of about 0.004.

	THF-P4	THF-P8	ACE-P4	ACE-P8
δ_m [MPa ^{0.5}]	20.46	20.99	20.98	21.33
v_m [cm ³ mol ⁻¹]	192.85	202.16	180.45	187.67
x_1 (sim)	0.68	0.66	0.63	0.61
A_1	3.13	-4.67	1.14	-5.03
B_1	-10.28	-0.42	-8.28	-0.06
A_2	5.85	6.26	6.44	6.48
B_2	-15.31	-15.72	-14.86	-14.90
A_{12}	7.42	7.51	7.79	7.50
ε_{ij} [kJ mol ⁻¹]	-22.79	-12.77	-20.74	-13.39
z_{FH}	6.63	6.89	6.90	6.87
χ_{FH}	-13.3	35.5	-7.42	34.37
$\Delta e_{m,z}$ (exp) [kJ mol ⁻¹]	-0.07	0.26	-0.03	0.25
$\Delta e_{m,FH}$ (exp) [kJ mol ⁻¹]	-0.13	0.35	-0.07	0.34

- 1 G. A. Mansoori, *Fluid Ph. Equilibria* 1993, **87**, 1-22.
- 2 I. Teraoka, in *Polymer Solutions: An Introduction to Physical Properties*, John Wiley & Sons, Inc., New York, 2002.
- 3 J. H. Hildebrand, in *The Solubility of Nonelectrolytes*, Dover Publications, Inc., New York, 1964.